Journal of Sound and Vibration (2000) **232**(5), 963–992
doi:10.1006/jsvi.1999.2779, available online at http://www.idealibrary.com on IDEAL®

EXPERIMENTAL IDENTIFICATION OF EXCITATION AND SUPPORT PARAMETERS OF A FLEXIBLE ROTOR–BEARINGS–FOUNDATION SYSTEM FROM A SINGLE RUN-DOWN

S. Edwards, A. W. Lees and M. I. Friswell

Department of Mechanical Engineering, University of Wales Swansea, Swansea, SA2 8PP, Wales

(*Received* 17 *September* 1999, *and in final form* 22 *November* 1999)

Field balancing of rotors with unknown foundation dynamics is more often than not a painstaking, time-consuming and expensive process. A recent method to identify both the excitation and flexible support parameters of a rotor-bearings-foundation system has been verified experimentally in this paper. In addition to mass unbalance, the excitation due to a bent rotor has been included in the method, which has great potential in the field, since it allows balancing to be performed using data obtained from just a single run-up or run-down. Using this single-shot balancing technique, vibration levels of an experimental rotor rig were successfully reduced to less than one-tenth of their original levels. The geometry of a bent rotor has also been accurately identified and it was shown that including bend identification in those cases where only unbalance forcing was present in no way detracted from the accuracy of the estimated unbalance or foundation parameters. The identification of the flexible foundation parameters was generally successful, with measured and estimated parameters matching very closely in most cases. The identification method was tested for a wide range of conditions, and proved suitably robust to changes in system configuration, noisy data and modelling error.

1. INTRODUCTION

Traditional turbogenerator balancing techniques require at least two run-downs, with and without the use of trial weights respectively, to enable the machine's state of unbalance to be accurately calculated [1]. In addition, for turbogenerator analysis purposes, accurate models of the flexible steel foundations used in modern power stations must be available, which is seldom the case, due to their complicated physical nature. Modelling techniques such as finite elements do not deliver acceptable results, and so direct estimation from measured response data has generally been accepted as the most promising technique [2]. It was shown [3] how it was possible to estimate both the flexible foundation parameters and the state of unbalance of a rotor, from a single set of vibration response data. This has obvious practical advantages for the efficient operation of turbomachinery. The only requirement of the method is a good rotor model, which is often available, or at least readily obtained using finite element modelling.

In this paper, the experimental verification of that method is described. The method has also been extended to include the identification of a bend in a rotor, as well as estimating the unbalance and flexible support parameters of the rotor-bearings-foundation system. The phenomenon of shaft forcing due to an initial bend has aroused interest over the last 20

0022-460X/00/200963 + 30 $35.00/0

years or so, albeit much less than mass unbalance. Bends in shafts may be caused in several ways, for example due to creep, thermal distortion or a previous large unbalance force. The forcing caused by a bend is similar, though slightly different, to that caused by conventional mass unbalance. There have been numerous cases in industry where vibration has been assumed to have arisen from mass unbalance and rotors have been balanced using traditional balancing procedures. This has repeatedly left engineers puzzled as to why vibration persists after balancing, and vibration levels may indeed even be worse than before balancing took place. Bend response is independent of shaft speed and causes different amplitude and phase angle relationships than is found with ordinary mass unbalance, where the forcing is proportional to the square of the speed [4, 5]. In the case of a bent rotor, the excitation is proportional to the magnitude of the bow along the rotor. A bent rotor gives rise to synchronous excitation, as with mass unbalance, and the relative phase between the bend and the unbalance casues different changes of phase angle through resonance than would be seen in the pure unbalance case, as described in references [4, 5]. It is therefore important to be able to diagnose a bend in a rotor from vibration measurements and thus distinguish between it and mass unbalance.

2. THEORY

Consider the system shown in Figure 1, where the rotor has both an unbalance and a bend. The system is written in terms of the dynamic stiffness matrices of its constituent components, as

$$\mathbf{Z}_R\mathbf{u}_R = \mathbf{f}_R \quad \text{for the rotor,} \tag{1}$$

$$\mathbf{Z}_B\mathbf{u}_B = \mathbf{f}_B \quad \text{for the bearings,} \tag{2}$$

$$\mathbf{Z}_F\mathbf{u}_F = \mathbf{f}_F \quad \text{for the foundations,} \tag{3}$$

where $\mathbf{Z}$ is the subscript-dependent dynamic stiffness matrix of the local system component, $\mathbf{u}$ is the subscript-dependent response vector and $\mathbf{f}$ is the subscript-dependent force, due to some excitation of the rotor. Subscripts R, B and F relate to the rotor, bearings and foundations respectively. The individual dynamic stiffness matrices of each of these

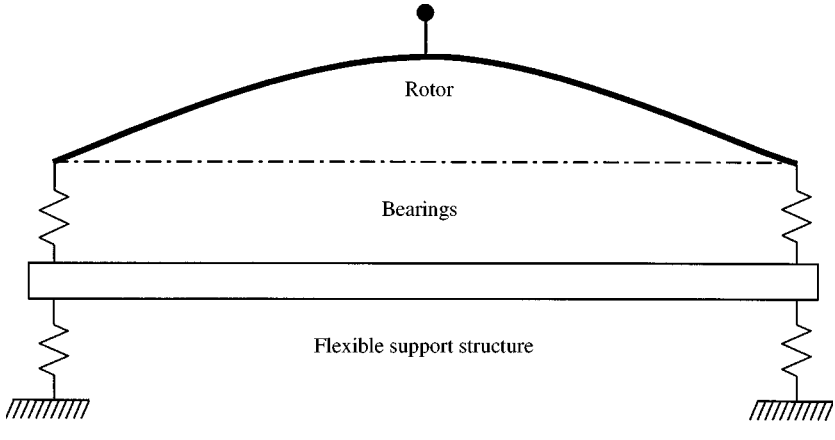

Figure 1. Rotor–bearings–foundation system with a bent rotor.

components are

$$\mathbf{Z}_R(\omega) = \mathbf{K}_R - \omega^2 \mathbf{M}_R, \tag{4}$$

$$\mathbf{Z}_B(\omega) = \mathbf{K}_B = \mathbf{B}, \tag{5}$$

$$\mathbf{Z}_F(\omega) = \mathbf{K}_F - \omega^2 \mathbf{M}_F + \mathrm{j}\omega \mathbf{C}_F, \tag{6}$$

where $\mathbf{K}$ is the subscript-dependent stiffness matrix, $\mathbf{M}$ is the subscript-dependent mass matrix, $\mathbf{C}_F$ is the foundation damping matrix and ω is the rotor running speed. The bearing model is restricted to direct stiffness terms for the sake of clarity. A speed-dependent bearing model with damping could also be included if required, as detailed in reference [3].

2.1. MODAL REPRESENTATION OF A ROTOR BEND

The rotor bend is expressed in terms of the free–free eigenvectors of the rotor, which are readily obtained from the numerical model. It is considered that, even for relatively simple systems with low numbers of modes, these modes will still be sufficient to adequately represent complicated bend geometry. The profile of the bend may be written, using this modal representation, as

$$\mathbf{s} = \mathbf{\Phi}\boldsymbol{\beta}, \tag{7}$$

where $\mathbf{s}$ is the profile of the bend along the length of the rotor, in two directions orthogonal to the rotor for the full two-directional case. If n modes are considered in the analysis then $\mathbf{\Phi}$ is a matrix of n column-vectors, where those vectors are the free–free eigenvectors of the rotor. The vector $\boldsymbol{\beta}(= \{\beta_1, \beta_2, \ldots, \beta_n\}^{\mathrm{T}})$ contains the corresponding n modal coefficients. The force due to the bend is then

$$\mathbf{f}_{bend} = \mathbf{K}_R \mathbf{s} = \mathbf{K}_R \sum_j \begin{Bmatrix} \boldsymbol{\phi}_{j,I} \\ \boldsymbol{\phi}_{j,B} \end{Bmatrix} \boldsymbol{\beta}_j, \tag{8}$$

where the first subscript j ($j = 1, 2, 3, \ldots, n$) refers to the particular mode being considered and the second subscript refers to either *internal* (I) or *connected* (B) degrees of freedom (d.o.f.) of the rotor. (Those d.o.f. of the rotor having no connection external to the rotor system are denoted as *internal* d.o.f.. The rotor is linked to the foundations via *connected* d.o.f., which are the points where the bearings are attached to the rotor and foundations respectively. It is assumed that the bearings can be adequately modelled using only these connected d.o.f.. In the case where the bearings are rigid (such as bush bearings or ball bearings), the connected d.o.f. link the rotor directly with the foundations. The foundations may or may not be specified with their own internal d.o.f., depending on the system in hand). $\boldsymbol{\phi}(= \boldsymbol{\phi}_1, \boldsymbol{\phi}_2, \boldsymbol{\phi}_3, \ldots, \boldsymbol{\phi}_n)$ are the corresponding mode shapes at the internal or bearing d.o.f., depending on the second subscript.

2.2. REPRESENTING THE SYSTEM

The three substructures are partitioned into their internal and connected d.o.f., giving

$$\begin{bmatrix} \mathbf{Z}_{R,II} & \mathbf{Z}_{R,IB} \\ \mathbf{Z}_{R,BI} & \mathbf{Z}_{R,BB} \end{bmatrix} \begin{Bmatrix} \mathbf{u}_{R,I} \\ \mathbf{u}_{R,B} \end{Bmatrix} = \begin{Bmatrix} \mathbf{f}_{R,I} \\ -\mathbf{f}_{F,B} \end{Bmatrix} + \mathbf{K}_R \mathbf{s}, \tag{9}$$

$$\begin{bmatrix} \mathbf{K}_B & -\mathbf{K}_B \\ -\mathbf{K}_B & \mathbf{K}_B \end{bmatrix} \begin{Bmatrix} \mathbf{u}_{R,B} \\ \mathbf{u}_{F,B} \end{Bmatrix} = \begin{Bmatrix} \mathbf{f}_{F,B} \\ -\mathbf{f}_{F,B} \end{Bmatrix}, \tag{10}$$

$$\begin{bmatrix} \mathbf{Z}_{F,BB} & \mathbf{Z}_{F,BI} \\ \mathbf{Z}_{F,IB} & \mathbf{Z}_{F,II} \end{bmatrix} \begin{Bmatrix} \mathbf{u}_{F,B} \\ \mathbf{u}_{F,I} \end{Bmatrix} = \begin{Bmatrix} \mathbf{f}_{F,B} \\ \mathbf{0} \end{Bmatrix}. \tag{11}$$

The second subscript I represents the internal d.o.f. of the rotor and foundations, depending on the first subscript, and the second subscript B represents the d.o.f. of the bearings. It is assumed that the force needed to give a relative bearing deflection is due to the relative displacement of $(\mathbf{u}_{R,B} - \mathbf{u}_{F,B})$, leading to the particular form of the bearing dynamic stiffness matrix in equation (10). In addition to the force produced by the bend, inclusion of the $\mathbf{f}_{R,I}$ term of equation (9) also permits specification of an unbalance forcing in the system. The force acting on the rotor due to unbalance excitation is of the form $\mathbf{f}_{R,I} = \mathbf{e}\omega^2$, where $\mathbf{e}$ is of the vector of unbalance magnitudes, containing non-zero components corresponding to the locations of eccentric mass on the rotor, acting at specified unbalance planes. Combining equations (9)–(11) leads to a general equation of motion for the global system:

$$\begin{bmatrix} \mathbf{Z}_{R,II} & \mathbf{Z}_{R,IB} & \mathbf{0} & \mathbf{0} \\ \mathbf{Z}_{R,BI} & \mathbf{Z}_{R,BB} + \mathbf{B} & -\mathbf{B} & \mathbf{0} \\ \mathbf{0} & -\mathbf{B} & \mathbf{B} + \mathbf{Z}_{F,BB} & \mathbf{Z}_{F,BI} \\ \mathbf{0} & \mathbf{0} & \mathbf{Z}_{F,IB} & \mathbf{Z}_{F,II} \end{bmatrix} \begin{Bmatrix} \mathbf{u}_{R,I} \\ \mathbf{u}_{R,B} \\ \mathbf{u}_{F,B} \\ \mathbf{u}_{F,I} \end{Bmatrix} = \begin{Bmatrix} \mathbf{f}_{R,I} \\ \mathbf{0} \\ \mathbf{0} \\ \mathbf{0} \end{Bmatrix} + \begin{Bmatrix} \mathbf{K}_R \begin{bmatrix} \boldsymbol{\Phi}_I \\ \boldsymbol{\Phi}_B \end{bmatrix} \boldsymbol{\beta} \\ \mathbf{0} \\ \mathbf{0} \end{Bmatrix} \tag{12}$$

or, in its simplest form

$$\mathbf{Z}\mathbf{u} = \mathbf{f}. \tag{13}$$

Equation (12) represents the general equation of motion for a rotor-bearings-foundations system of this type. If further refinements, such as any particular gyroscopic or damping effects are to be included in the model then the only modifications that need to be made are in the specification of the individual dynamic stiffness matrices in equations (4)–(6). In the present study, the foundations are not specified as having any internal d.o.f., and the ball bearings used for the experimental rig are considered rigid (infinite stiffness), reducing equation (12) to

$$\begin{bmatrix} \mathbf{Z}_{R,II} & \mathbf{Z}_{R,IF} \\ \mathbf{Z}_{R,FI} & (\mathbf{Z}_{R,FF} + \mathbf{Z}_F) \end{bmatrix} \begin{Bmatrix} \mathbf{u}_{R,I} \\ \mathbf{u}_{R,F} \end{Bmatrix} = \begin{Bmatrix} \mathbf{f}_{R,I} \\ \mathbf{0} \end{Bmatrix} + \begin{bmatrix} \mathbf{K}_{R,II} & \mathbf{K}_{R,IF} \\ \mathbf{K}_{R,FI} & \mathbf{K}_{R,FF} \end{bmatrix} \begin{bmatrix} \boldsymbol{\Phi}_I \\ \boldsymbol{\Phi}_F \end{bmatrix} \boldsymbol{\beta}. \tag{14}$$

The rotor stiffness matrix, $\mathbf{K}_R$, has now been partitioned into internal and connected d.o.f., subscript F has replaced subscript B, since the rotor now connects directly with the foundations, and the terms relating to the internal d.o.f. of the foundations have been discarded, since these are no longer of interest.

2.3. IDENTIFYING THE SYSTEM

The top set of terms in equation (14) yields an expression for $\mathbf{u}_{R,I}$, which is then eliminated from the bottom set, allowing these terms to be rewritten with the unknown and known terms grouped on the left- and right-hand side respectively, giving

$$\begin{aligned} &\mathbf{Z}_F\mathbf{u}_{R,F} + [\mathbf{Z}_{R,FI}\mathbf{Z}_{R,II}^{-1}\mathbf{K}_{R,II}\boldsymbol{\Phi}_I + \mathbf{Z}_{R,FI}\mathbf{Z}_{R,II}^{-1}\mathbf{K}_{R,IF}\boldsymbol{\Phi}_F - \mathbf{K}_{R,FI}\boldsymbol{\Phi}_I - \mathbf{K}_{R,FF}\boldsymbol{\Phi}_F]\boldsymbol{\beta} \\ &\quad + \mathbf{Z}_{R,FI}\mathbf{Z}_{R,II}^{-1}\mathbf{f}_{R,I} = [\mathbf{Z}_{R,FI}\mathbf{Z}_{R,II}^{-1}\mathbf{Z}_{R,IF} - \mathbf{Z}_{R,FF}]\mathbf{u}_{R,F}. \end{aligned} \tag{15}$$

Now let

$$[\mathbf{Z}_{R,FI}\mathbf{Z}_{R,II}^{-1}\mathbf{Z}_{R,IF} - \mathbf{Z}_{R,FF}]\mathbf{u}_{R,F} = \mathbf{P}, \tag{16}$$

$$[\mathbf{Z}_{R,FI}\mathbf{Z}_{R,II}^{-1}\mathbf{K}_{R,II}\mathbf{\Phi}_I + \mathbf{Z}_{R,FI}\mathbf{Z}_{R,II}^{-1}\mathbf{K}_{R,IF}\mathbf{\Phi}_F - \mathbf{K}_{R,FI}\mathbf{\Phi}_I - \mathbf{K}_{R,FF}\mathbf{\Phi}_F] = \mathbf{Q}. \tag{17}$$

and

$$\mathbf{Z}_{R,FI}\mathbf{Z}_{R,II}^{-1}\mathbf{f}_{R,I} = \mathbf{Z}_{R,FI}\mathbf{Z}_{R,II}^{-1}\omega^2\mathbf{e} = \mathbf{Re}, \tag{18}$$

where **P**, **Q** and **R** contain terms collected at all measured frequencies. Substituting the unknown mass and stiffness parameters of equation (6) for $\mathbf{Z}_F$ in equation (15) allows these desired elements to be estimated in a least-squares sense. If the unknown parameters are grouped into a vector **v**, and a corresponding matrix $\mathbf{w}(\omega)$ containing the related response terms at each measured frequency is also defined, then we have

$$\mathbf{Z}_F(\omega)\mathbf{u}_{R,F}(\omega) = \mathbf{w}(\omega)\mathbf{v}. \tag{19}$$

The parameters contained in **v** depend on the form of the dynamic stiffness matrix specified for the foundations and the ordering of these parameters may be designated as desired. The foundation model used for these experiments was initially specified as diagonal mass, damping and stiffness matrices (i.e., with no cross-coupling present), giving

$$\mathbf{w}(\omega)\mathbf{v} = \begin{bmatrix} u_{Ax} & 0 & 0 & 0 & -\omega^2 u_{Ax} & 0 & 0 & 0 & \mathrm{j}\omega u_{Ax} & 0 & 0 & 0 \\ 0 & u_{Ay} & 0 & 0 & 0 & -\omega^2 u_{Ay} & 0 & 0 & 0 & \mathrm{j}\omega u_{Ay} & 0 & 0 \\ 0 & 0 & u_{Bx} & 0 & 0 & 0 & -\omega^2 u_{Bx} & 0 & 0 & 0 & \mathrm{j}\omega u_{Bx} & 0 \\ 0 & 0 & 0 & u_{By} & 0 & 0 & 0 & -\omega^2 u_{By} & 0 & 0 & 0 & \mathrm{j}\omega u_{By} \end{bmatrix} \begin{Bmatrix} k_{Ax} \\ k_{Ay} \\ k_{Bx} \\ k_{By} \\ m_{Ax} \\ m_{Ay} \\ m_{Bx} \\ m_{By} \\ c_{Ax} \\ c_{Ay} \\ c_{Bx} \\ c_{By} \end{Bmatrix}. \tag{20}$$

This was considered a realistic representation of the physical system in question, where k, m and c are the stiffness, mass and damping values of the foundations. The first subscript refers to either foundation A (drive-side) or foundation B and the second subscript refers to either the horizontal (x) or vertical (y) direction. Equation (15) is now rewritten using equations (16)–(18) and (20) as

$$\mathbf{Wv} + \mathbf{Re} + \mathbf{Q}\boldsymbol{\beta} = \mathbf{P} \tag{21}$$

leading to the solution of

$$[\mathbf{W}\ \mathbf{R}\ \mathbf{Q}]\begin{Bmatrix}\mathbf{v}\\ \mathbf{e}\\ \boldsymbol{\beta}\end{Bmatrix} = \mathbf{P}. \tag{22}$$

This is for the most general case, with the force on the rotor due to both bend and unbalance excitation. If either of these excitation sources is omitted from the analysis, the same methodology applies, only without the respective forcing terms, leading to the estimation equations of

$$[\mathbf{W}\ \mathbf{R}]\begin{Bmatrix}\mathbf{v}\\ \mathbf{e}\end{Bmatrix} = \mathbf{P}, \tag{23}$$

$$[\mathbf{W}\ \mathbf{Q}]\begin{Bmatrix}\mathbf{v}\\ \boldsymbol{\beta}\end{Bmatrix} = \mathbf{P}, \tag{24}$$

for excitation due solely to unbalance and bend respectively. Note that the terms relating to the foundation parameter identification do not change in any way.

The condition of the matrices to be inverted in equations (22)–(24) should be taken into account, and the condition number may be improved by pre-conditioning or by scaling of parameters. In addition, if *a priori* knowledge of some terms exists, such as one or more of the foundation mass or stiffness terms, then this information may be included in the analysis. For further detail on both of these issues, see reference [3]. In the present study, solutions to equations (22)–(24) were obtained using the least-squares method. Singular-value decomposition (SVD) methods [6] may prove beneficial in cases where there is not enough information to sufficiently identify all desired parameters, although this was not necessary here. In practical cases, **W**, **Q** and **P** will be complex, in which case these matrices must be separated into their real and complex parts, leading to a doubling of the order of these terms, although the parameters it is intended to identify remain real.

3. THE EXPERIMENTAL ROTOR RIG

3.1. MECHANICAL HARDWARE

A general view of the experimental rig is shown in Figure 2. The whole apparatus was mounted on a massive, rigid steel table. The steel baseplate measured $1100 \times 300 \times 11$ mm with a 16 mm wide central slot to allow for fixing of support frames and disk guards, and with holes allowing both the motor and the support blocks to be attached to the plate. To ensure the plate remained rigid, it was supported by 3 steel blocks of size $50 \times 300 \times 100$ mm. At both ends and near the middle, the baseplate was tightened down onto these blocks. Clamps were then used to ensure that the plate remained rigid relative to the table. The rotor was driven by a 0·55 kW permanent magnet DC motor, with a maximum speed of 3000 r.p.m. A thyristor motor-controller provided the necessary voltage supply to the motor. Solid silver-steel shafts of diameter 12 mm and length 750 mm were used, along which balance disks of inside diameter 12 mm, outside diameter 74 mm and thickness 15 mm could be fixed at any desired point. There were 16 equally spaced M4-threaded holes in each disk at radii of 30 mm, to allow for the addition of balance weights. A flexible coupling was used, which helped to compensate for any misalignment between the bearings

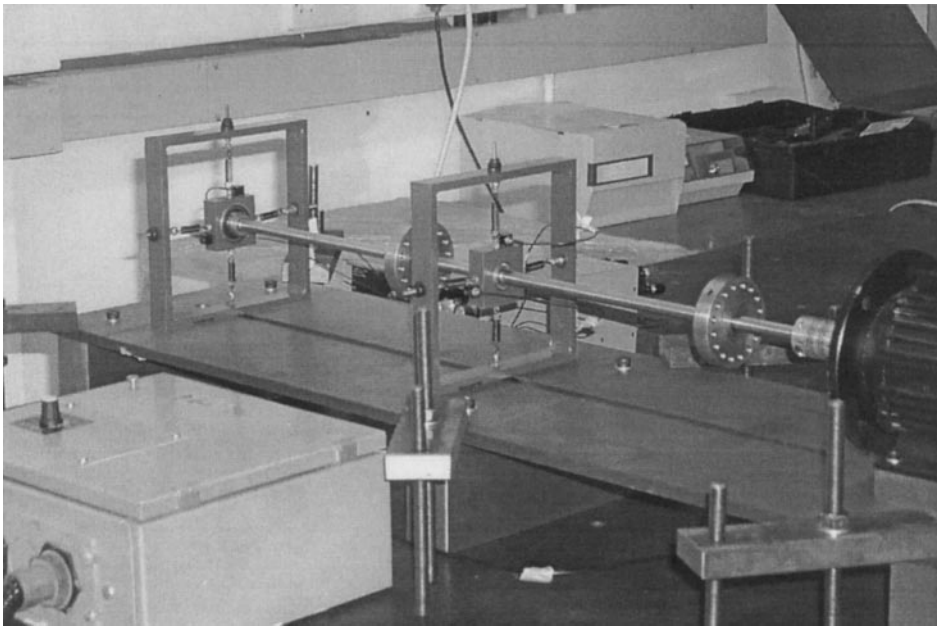

Figure 2. General view of experimental rotor rig.

and/or motor, as well as preventing any unwanted dynamic effects occurring in the motor being transmitted through the coupling into the rotor itself.

Figure 3 shows a view of one of the two flexible support units, and the bearing and housing being supported. Both devices were built to the same specifications. The rotor ran in parallel outer-diameter, self-lubricating ball bearings, having an extended inner race to permit the necessary grub-screw fixing to the shaft. For analysis purposes these bearings were considered rigid. The bearings were housed within square steel blocks of size 50×50 mm and thickness 19 mm. The outer frame seen in Figure 3 was rigidly fixed to the baseplate by means of a bolt passing through the central slot in the baseplate. In order to reproduce the type of dynamic behaviour present in a real machine mounted on flexible foundations, it was necessary for the connection between the bearing and the outer frame (which is analogous to the physical earth of the foundations in a real machine) to be flexible. This flexibility was introduced by the use of steel extension springs. The springs were connected to the outer frame using M4 bolts of length 40 mm, with plain washers welded to the bolt heads, to which the springs were attached. These bolts were long enough to pass through holes in the frame and were tightened against the inside of the frame using a nut and thin rubber washer, and against the outside using dampers. Damping was introduced into the flexible supports on the top and sides of the frame by using neoprene M4 anti-vibration fasteners on the outside of the frame.

To verify the identification method to be tested using this experimental apparatus, it was necessary to know the values of the foundation masses and stiffnesses it was intended to identify. The required mass was that of the bearing, housing, accelerometers and a portion of the spring mass. The effect of the accelerometer cable was considered negligible. The most straightforward way to determine the support stiffness was to perform an impact test on the support unit, without the rotor in place and whilst rigidly bolted to the baseplate. The measured natural frequency was then used in conjunction with the measured mass to

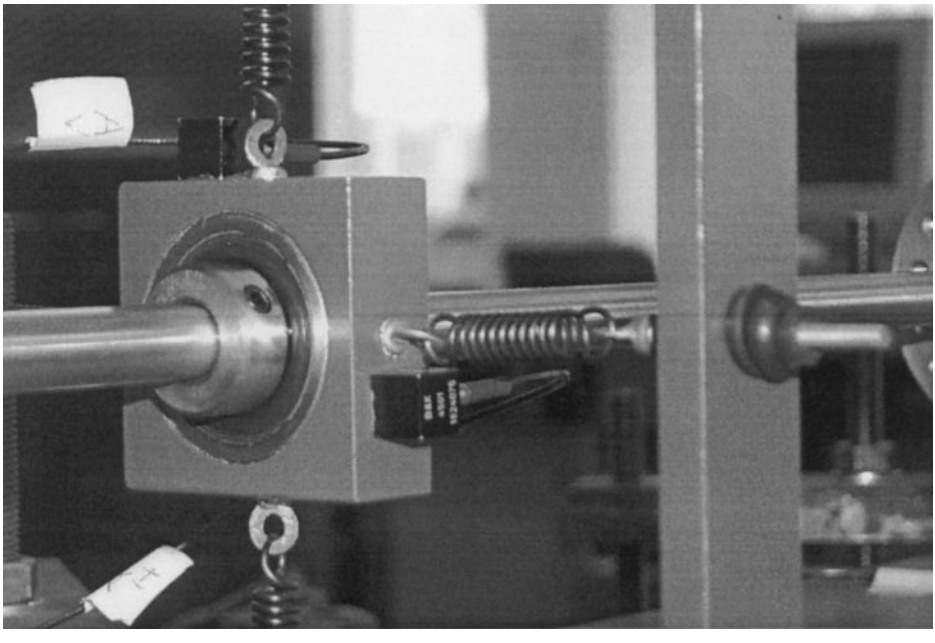

Figure 3. Detail of bearing, flexible support and accelerometer mountings.

TABLE 1

Measured foundation parameters

Property	Foundation	Direction	Measured value
Mass (kg)	A	x	0·356
		y	0·356
	B	x	0·352
		y	0·352
Stiffness (N/m)	A	x	17 212
		y	17 707
	B	x	17 277
		y	17 523

calculate the support stiffness in the direction being measured. This test was performed for both support units and in both directions. The results of these tests are given in Table 1, where A and B refer to the drive-side and free-end of the rotor respectively.

The whole bearing/support arrangement was designed to allow adjustment of the distance between the bearing housing and the outer frame. This was important for alignment of the rotor, as well as for applying pre-tension to the springs. Adjustment was achieved by loosening both the nut on the inside of the frame and the damper on the outside of the frame, altering the position of the M4 bolt until the correct alignment or desired pre-tension was attained, and finally tightening both the nut and the damper against the body of the frame. The rotor rig required manual alignment: a digital height gauge was used for vertical adjustment and digital calipers for horizontal adjustment. Although perfect

alignment could not be hoped for using this method, a value lower the maximum allowable coupling misalignment of 0·13 mm was satisfactorily obtained.

3.2. DATA ACQUISITION AND SIGNAL PROCESSING

The identification method detailed above requires frequency-based measurements of the rotor response measured at the bearing housings, over a controlled run-up or run-down of the machine. The objective of the measurement system was therefore to return a first-order response, as only synchronous excitation was being investigated, of the rotor over this controlled period. Brüel and Kjaer Type 4501 cubic accelerometers were used to measure the accelerations of the bearing housings. Measurements were taken at both bearings in both the horizontal and vertical directions. These general-purpose piezoelectric accelerometers were advantageous for the present study due to their small size ($10 \times 10 \times 10$ mm) and low mass (3.5 g). A four-channel D.J. Birchall CA/04 charge amplifier converted the piezoelectric charge produced by the accelerometers into a low impedance voltage of required magnitude. In order to perform the signal processing required for these experiments, a reference signal was necessary. This reference, or tachometer, signal allows the angular position of the rotor to be known relative to a constant location on the shaft. Here, the rotation of a single keyway cut into the rotor was detected by a proximity sensor, providing a once-per-revolution output pulse upon the passing of the edge of the keyway. The width of the keyway and the rate at which the tachometer sensor data was sampled was such that the maximum possible angular delay in the output signal was 7.2° (a 2% error). This was for the maximum speed of 3000 r.p.m. and for the worst case where the passing of the keyway edge was only just missed by the previous data sample. This maximum possible error was deemed acceptable, considering the fact that the rotor would not normally be run at full speed, the probability of a sample just missing the passing of the keyway edge was relatively low, and because of the averaging effect introduced by processing. The influence of this error on the overall analysis was not considered significant.

A general-purpose PC-based data acquisition card, integrated into a Pentium 90 PC, with 16 MB of RAM and 426 MB of hard-disk space was used for both motor control and data acquisition. The constant sample rate of 2500 Hz was used to acquire the tachometer and accelerometer signals. This high acquisition rate was used since there were no anti-aliasing filters in place. Given the four channels of time-domain response data and the tachometer signal stored, signal processing was performed on these data to extract the required first order response. For both bearings and in both directions, complex vectors of measured displacements could then be grouped into a matrix. This matrix of displacement vectors, corresponding to the term $\mathbf{u}_{R,F}$ in equation (14), was then used in the identification method.

3.3. ROTOR MODEL USED FOR CALCULATIONS

For the majority of results presented in this paper, the system was configured in such a way that, measured from the coupling, disks A and B were at distances of 79 and 459 mm respectively, whilst bearings A and B were at distances of 234 and 733 mm. A schematic diagram of the rotor model is shown in Figure 4, where m_c and k_c refer to the mass and stiffness of the flexible coupling respectively. The corresponding model details are given in Table 2, where it can be seen that the rotor model consisted of five two-noded beam elements representing the shaft, each node having two translational and two rotational d.o.f. The two disks were modelled using additional mass and inertia terms at the disk locations.

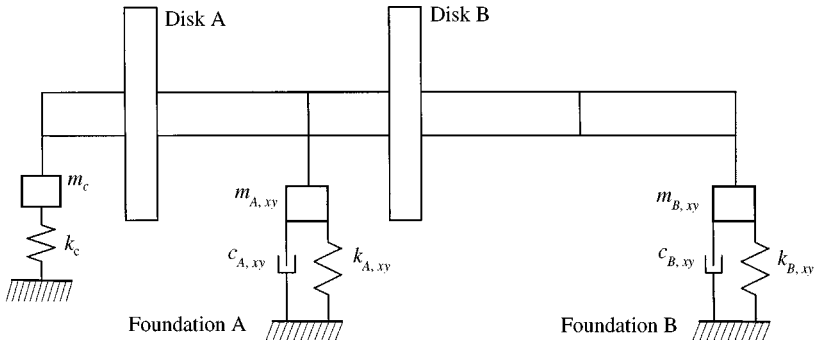

Figure 4. Schematic diagram of rotor model.

TABLE 2

Details of rotor model

Station	Distance from coupling (mm)	Element length (mm)
1. (coupling)	0	—
2. (disk A)	79	79
3. (bearing A)	234	155
4. (disk B)	459	225
5.	596	137
6. (bearing B)	733	137

The free–free rotor model was verified by performing impact tests on the rotor supported in elastic slings. The first four measured and predicted (in brackets) natural frequencies were: two rigid-body modes, 77·5 (77·5) and 211·3 (215·2) Hz. This error was not considered significant. The modelling of the flexible coupling was achieved using a combination of engineering judgement and experiment. Half of the mass of the coupling was used for the model and an initial estimate made of the coupling lateral bending stiffness. A hammer test was then performed on the global system. The eigenfrequencies of the system were calculated, using the rotor model including the estimated coupling mass and stiffness values, together with the previously measured foundation parameters, and compared to those measured from the test. A value of 9000 N/m was found to be the optimum stiffness for the coupling, in terms of comparing measured and estimated natural frequencies.

4. EXPERIMENTAL RESULTS

Since this was the first time that the identification method had been tested experimentally, the potential of the rotor rig to quickly deliver reliable and repeatable results was utilized, and many run-downs were performed on which the identification method was carried out. The identification of the flexible foundations and unbalance excitation alone was performed for various unbalance, rotor and foundation configurations. A bent rotor was also used experimentally and identified in conjunction with unbalance

excitation and the model of the supporting structure. The specification of various foundation parameter sets has also been investigated.

4.1. IDENTIFICATION RESULTS: INITIAL ROTOR CONFIGURATION

For the set of results described in this section, only the unbalance configuration of the rotor was changed, by adding extra mass to the disks. The actual rotor configuration described above remained the same throughout, and the reference speed range of 45–15 Hz was used for all runs. The state of unbalance on the rig for each run is given in Table 3, together with the identified unbalance parameters. Since the foundations were not changed in any way throughout the acquisition of these results, the estimated foundation parameters were expected to remain constant. The mean values and standard deviations of the estimated foundation parameters are given in Table 4, together with their measured values, for purposes of comparison. The values of unbalance mass used were of similar magnitude to the residual unbalance of the rotor. Note that the results for run 20 were not taken into account when calculating the mean values—the machine was so well-balanced in this case that there was insufficient forcing to allow reasonable estimates to be calculated. This particular case is discussed in more detail later.

Excellent accuracy in the identification of the unbalance parameters was achieved. The residual unbalance estimates for runs 1, 2 and runs 3–7 are consistent, with no significant discrepancy in either unbalance magnitude or angle. The change in residual unbalance between runs 2 and 3 was due to the fact that the rotor was taken apart and put back together again at this point. This consistent identification highlights the robustness of the identification method for dealing with different data sets. The results for runs 3–20, with many variations in unbalance configuration, are also extremely encouraging. The most straightforward way to check the accuracy of the unbalance estimates was to calculate the error between the estimated additional unbalance (calculated using the estimated unbalance from two consecutive runs) and the actual additional unbalance. With the exception of run 12, where the maximum error in magnitude is 0·6 g for disk A, all other magnitude errors are no greater than 0·3 g, which is generally very low compared to the magnitude of the added masses. The means and standard deviations of the estimated errors are both 0·1 g. Likewise, the errors in unbalance angle are also very small, with the mean error of 17° being less than 5% of a revolution. These low errors in estimated unbalance are considered acceptable.

It should first be noted that (as stated above), the reason for the poor foundation estimates for run 20 was because the machine was so well-balanced in this case that there was insufficient forcing to allow reasonable estimates to be calculated. However, it should not be overlooked that the error in estimated added unbalance is still very low for this case. The maximum error in foundation stiffness estimation was just 6%, compared to the measured values, for the vertical direction at foundation A. The mass identification exhibits similar behaviour in terms of consistency, with the largest variation in estimates being for foundation A. Here, the mean estimated mass for foundation A is less accurate then for foundation B. Errors of 28 and 35% arise for the horizontal and vertical directions respectively, compared to just 3 and 0% for foundation B. The reason why the stiffness estimation is more robust than the mass estimation may be due to the fact that the identified mass terms are proportional to the square of the frequency, and so are weighted more towards higher frequencies, whilst the stiffness identification is equally weighted over all frequencies. However, the reason why the identification of foundation A suffers more than foundation B is less clear. The most probable cause is that foundation A is nearest the coupling, and any error in the modelling of the coupling is likely to have a much stronger

TABLE 3

Actual and estimated unbalance parameters

Run	Unbalance (disk A; disk B) (mass (g) @ phase angle (deg))			
	Unbalance configuration	Estimated unbalance	Calculated addition	Error
1	Residual Residual	1·3@174 1·8@97		
2	Residual Residual	1·3@173 1·8@96		
3	Residual Residual	0·6@116 1·7@100		
4	Residual Residual	0·6@121 1·7@99		
5	Residual Residual	0·6@120 1·7@99		
6	Residual Residual	0·6@120 1·7@99		
7	Residual Residual	0·6@119 1·7@98		
8	0·8@120 2·4@100	1·5@122 4·2@116	0·9@127 2·6@125	0·1@7 0·2@25
9	Residual Residual	0·8@118 1·7@97	0·7@308 2·6@308	0·1@8 0·2@28
10	Residual 2·4@90	0·9@114 4·2@102	0·1@81 2·5@105	— 0·1@15
11	Residual Residual	0·7@114 1·8@97	0·1@290 2·5@285	— 0·1@15
12	2·0@312 2·4@263	1·9@ − 77 0·8@ − 44	2·6@286 2·5@289	0·6@ − 26 0·1@26
13	Residual Residual	1·2@ − 163 1·8@97	2·3@137 2·6@109	0·3@5 0·2@26
14	2@281 2@281	2·3@ − 91 1·0@6	2·3@300 2·1@306	0·3@19 0·1@25
15	Residual Residual	1·4@ − 160 1·8@95	2·2@124 2·1@124	0·2@23 0·1@23
16	2@349 2@259	1·0@ − 11 0·2@ − 10	2·3@6 1·9@282	0·3@17 −0·1@23
17	Residual Residual	1·2@ − 163 1·8@94	2·2@183 1·9@101	0·2@14 −0·1@22
18	1·2@11 1·8@281	0·2@68 0·9@26	1·3@24 1·7@304	0·1@13 −0·1@23
19	Residual Residual	0·2@ − 162 1·8@95	1·3@205 1·7@125	0·1@14 −0·1@24
20	1·2@11 1·8@259	0·2@86 0·2@34	1·3@25 1·7@281	0·1@14 −0·1@22

TABLE 4

Identified foundation parameters

Estimated parameter	Foundation/direction (measured value)	Estimated mean value (S.D.)	Error (%)
Stiffness (N/m)	Ax (17 212)	17 015 (538)	−1
	Ay (17 707)	18 797 (515)	6
	Bx (17 277)	16 691 (211)	−3
	By (17 523)	16 589 (148)	−5
Mass (kg)	Ax (0·356)	0·455 (0·012)	28
	Ay (0·356)	0·480 (0·013)	35
	Bx (0·352)	0·361 (0·005)	3
	By (0·352)	0·352 (0·005)	0
Damping (N s/m)	Ax	5·89 (1·60)	–
	Ay	−5·77 (1·88)	–
	Bx	0·30 (0·82)	–
	By	3·02 (0·65)	–

influence on that foundation which is closest. In addition, if there are any dynamic effects due to the motor, which is not included in the rotor model, then these may also have a part to play. The accuracy of the estimated damping parameters is less straightforward to judge, since the actual foundation damping is unknown. However, the same trend of larger standard deviations for foundation A is evident, and the low magnitudes of the estimated damping coefficients (3.3, −3.0, 0.2 and 2.0% for Ax, Ay, Bx, By) would be expected for a structure of this type. The reason for the negative damping parameter for the vertical direction of foundation A may be due to some underlying physical cause or again due to some kind of modelling error. This does not, however, give cause for concern, as the magnitudes of the damping parameters are indeed very low.

Overall, both the foundation and the unbalance parameters have been estimated to a high degree of accuracy. The robustness of the method to changes in excitation has been shown by the consistently accurate foundation parameter identification and highly accurate unbalance identification, with various unbalance configurations being used. Although the estimates for foundation A are the least accurate, the estimates for foundation B and the unbalance estimates do not appear to suffer as a result. This shows great promise for the method in terms of application to real machines, where some kind of modelling error is normally inevitable. Robustness to this type of error, as seen in this instance, is therefore highly desirable.

A final check to be made on the estimated parameters was to combine them with the rotor model to obtain the estimated system responses, and to compare these estimated responses with those measured at the bearing housings, where a close fit between estimated and measured responses is indicative of a successful identification. This has been done in Figure 5, for the parameters identified from run 8. This particular set of data was simply chosen as an example and is typical of the estimated responses obtained for all other data sets considered here. As would be expected from the accurate parameter identification discussed above, there is excellent agreement between measured and estimated responses. The only discrepancy of any significance is found between the estimated and measured responses in the vertical directions of both bearings, at the lower critical speed. The reason for this is most likely the negative damping coefficient identified in the vertical direction of bearing A.

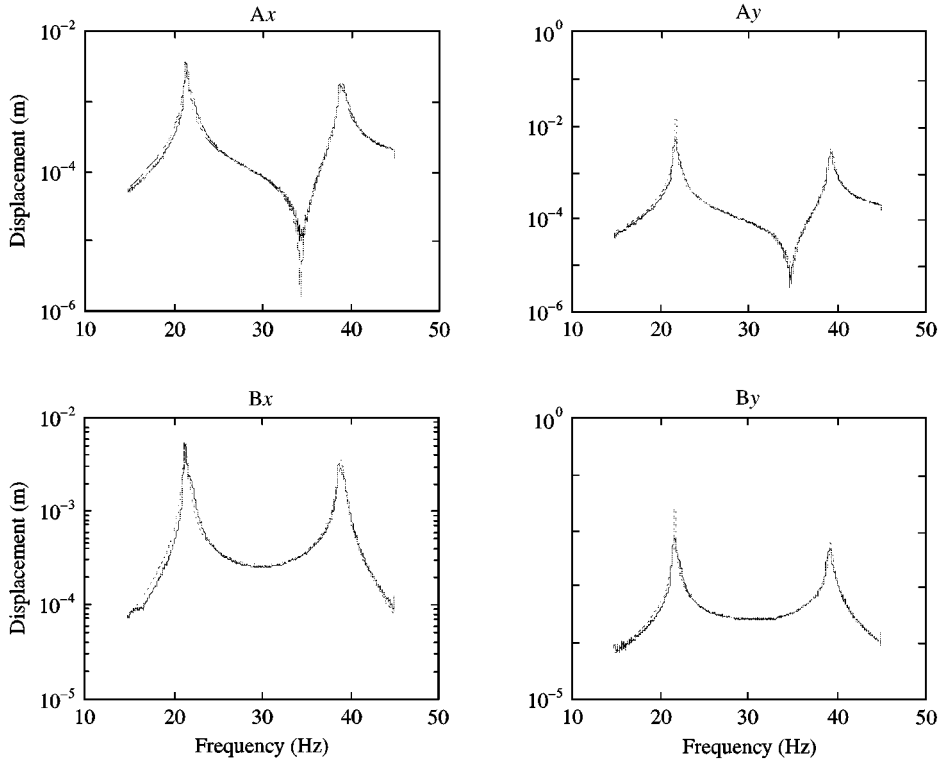

Figure 5. Measured and estimated responses (pk-pk) for run 8. ——, measured; – – –, estimated.

Since one of the main goals of this work was to reduce vibration levels of rotating machinery by performing balancing using a single set of data, balancing was carried out using the identified parameters obtained from run 19. The identified unbalance masses were placed at positions opposite (as far as the disks would allow) the identified unbalance angle. The responses obtained for the two runs are shown in Figure 6. The responses are plotted using a linear scale as this allows a clearer comparison of the response magnitudes to be made. It can be seen from Figure 6 that the balancing procedure carried out on the machine was highly successful. Vibrational amplitude at the lower critical speed was reduced by up to 92%, whilst at the higher critical speed the amplitude was reduced by a maximum of 58%. The lowest measured reduction was 50%, for the higher critical speed in the vertical direction at both bearings. These large reductions in amplitude represent a very significant improvement in the machine's dynamic behaviour. The very low response amplitudes for run 20 are the reason why the estimated foundation parameters are of poor quality. Indeed, much of the measured response is low enough to be masked with noise.

The flexible support and unbalance identification method has thus far been applied to numerous sets of data obtained in experiment. The identified parameters were shown to be highly accurate and robust to changes in unbalance configuration and possible modelling error. Confidence acquired from the identification results was applied to perform balancing on the experimental rotor rig, whereby large reductions in vibrational amplitude were achieved after balancing from a single run-down. As far as field balancing is concerned, if it were possible to obtain such reductions in vibration from only a single run-down of a machine, as has been achieved here, then this would be a great benefit for machinery operation.

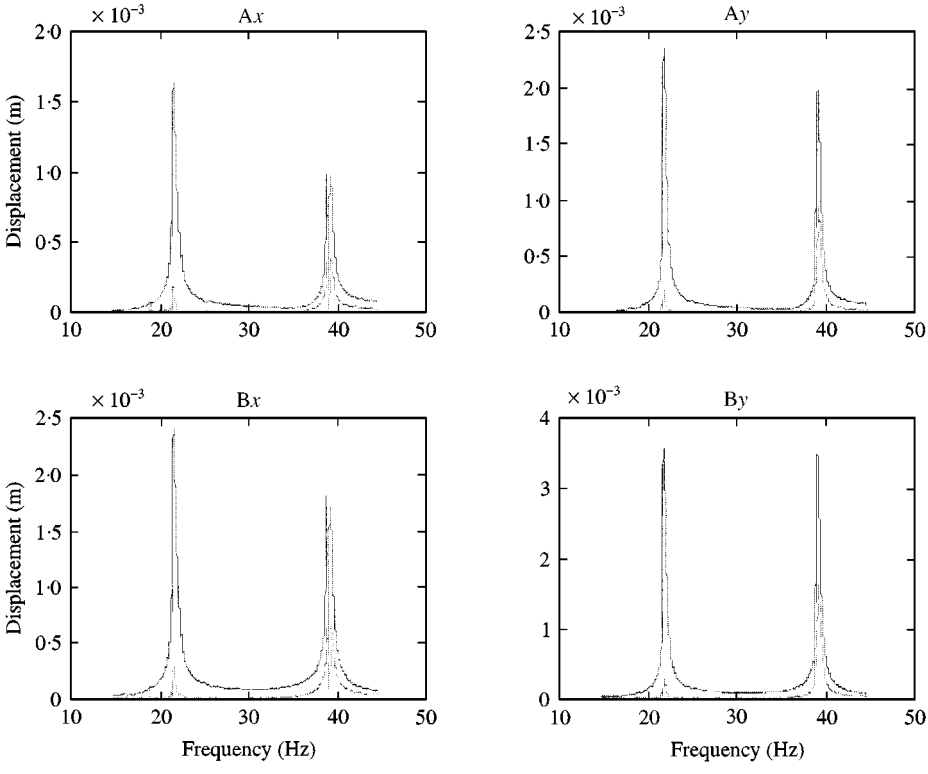

Figure 6. Measured responses (pk-pk) before and after balancing. ——, before; – – –, after.

4.2. IDENTIFICATION RESULTS: CHANGES IN SYSTEM CONFIGURATION

To examine the robustness of the identification method to changes in the system, several run-downs were performed using different configurations. A fully demanding set of conditions was chosen, including a lack of information to be used for the identification, poor selection of balance planes, and also physical changes in foundation parameters. This section is divided into two subsections, the first dealing with the changes made to the rotor and the second discussing the changes made to the foundations.

4.2.1. *Different rotor configurations*

Run-downs were performed for various rotor and unbalance configurations. The system configuration for each run is given in Table 5, together with the identified unbalance parameters. Figure 7 shows the relative positions of the bearings and disks for the different rotor configurations C1 to C4, and the two critical speeds present in each case. The reference frequency range of 45–15 Hz was used for all runs except for configuration 4, where an upper limit of either 40 or 50 Hz was used, as stated in the table. The mean values, standard deviations and errors between estimated and measured foundation parameters are listed in Table 6.

The parameters identified from configurations C1 to C3 show little discrepancy with the known unbalance or foundation parameters. For unbalance, the maximum error in added unbalance magnitude is 0·2 g for C3, whilst there is no significant error in identified unbalance magnitude for either C1 or C2. The maximum error in unbalance angle is just 44°

TABLE 5

System configurations and identified unbalance parameters

Run	Unbalance (disk A; disk B) (mass (g) @ phase angle (deg))			
	Unbalance configuration	Estimated unbalance	Calculated addition	Error
Rotor configuration 1				
1	Residual	0·4@63		
	Residual	1·3@94		
2	0·4@236	0·2@0	0·4@280	0·0@44
	1·2@281	0·6@33	1·2@300	0·0@19
Rotor configuration 2				
3	Residual	0·7@65		
	Residual	2·1@93		
4	0·8@236	0·1@ − 60	0·8@252	0·0@16
	2·0@281	0·9@22	2·0@299	0·0@18
Rotor configuration 3				
5	Residual	0·6@ − 69		
	Residual	2·2@91		
6	0·8@124	0·0@ − 107	0·6@113	−0·2@ − 11
	2·0@281	0·8@40	1·8@292	−0·2@11
Rotor configuration 4				
7	Residual	13·0@ − 61		
40 Hz	Residual	15·9@112		
8	Residual	5·2@ − 33		
50 Hz	Residual	7·5@124		
9	4·8@144	6·9@148	12·1@148	7·3@4
50 Hz	7·0@304	7·4@ − 25	14·4@320	7·4@16
10	4·8@144	6·6@147	11·8@147	6·6@3
50 Hz	7·0@304	7·2@ − 25	14·2@320	7·0@16
11	Residual	5·5@ − 47	12·0@321	7·2@ − 3
50 Hz	Residual	8·2@116	14·5@134	7·5@10

(12%) for run 2. The foundation parameters are also estimated to a high degree of accuracy. For stiffness, the mean values and standard deviations (in parentheses) for the six runs with C1 to C3 are 16 154 (718), 18 294 (526), 16 702 (173) and 16 747 (77) N/m for Ax, Ay, Bx and By, corresponding to very low errors in stiffness estimation of −6, 3, −3 and −4% respectively. Mass estimation is also accurate, where the means and standard deviations for these runs are 0·432 (0·015), 0·460 (0·014), 0·360 (0·007) and 0·355 (0·005) g, giving errors of 21, 29, 2 and 1% respectively. For damping estimation, similar behaviour to that described in the previous section was exhibited, with mean values and standard deviations of 4·90 (2·35), −0·82 (5·15), −0·22 (1·02) and 1·85 (1·86) N s/m. Again, these damping estimates are very low.

Some interesting and important points for the identification method are apparent from the identification performed using configuration C4, where the distance between the two disks was only 1·0 mm and the higher critical speed was 44 Hz. For run 7, where the 40 Hz

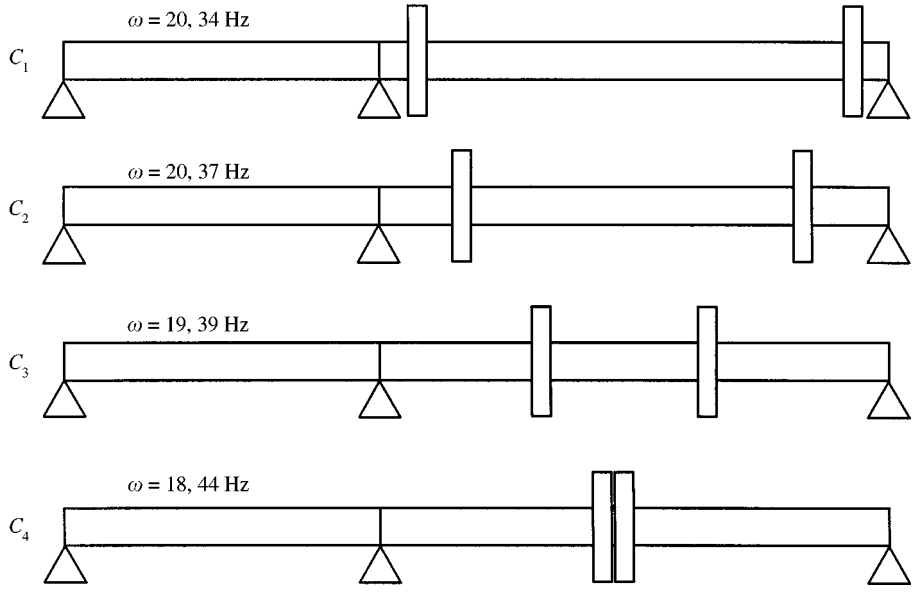

Figure 7. Rotor configurations used for system identification.

running range of the rotor did not include this higher critical speed, both the unbalance and foundation estimates suffer as a direct consequence. The residual unbalance estimates of 13·0 and 15·9 g for disks A and B respectively are obviously highly overestimated, when compared to the magnitudes of residual unbalance estimated from previous runs. Note also the 180° phase difference between the unbalance estimates for the two disks. The foundation stiffness and mass estimates for this run are 13 103, 13 768, 18 445, 18 116 N/m (stiffness) and 0·130, 0·064, 0·526 and 0·479 g (mass) for Ax, Ay, Bx and By respectively. Whilst the errors in stiffness for this run of -24, -22, 7 and 3% are not considered unacceptable, the errors in mass of -63, -82, 49 and 36% are indeed of poor quality. Once the higher critical speed was included in the 50 Hz range used for run 8, the errors between identified and measured stiffness and mass parameters fell to -13, -1, -2 and -3% (stiffness) and -9, 3, 17 and 13% (mass). The magnitudes of these errors are similar to those obtained from previous runs and are considered acceptable. The difference in errors between the foundation estimation for the case where the second critical speed is included, and that where it is not, show that the foundation identification suffered in the latter case due to a lack of information. Once this extra information was included, the estimated foundation parameters then became accurate. This is not, however, the case for the unbalance estimation. For runs 9–11, although the identified foundation parameters were consistently accurate, the estimated unbalance parameters were not. Large errors in added unbalance magnitude are evident for these runs, although the estimated unbalance angles remain accurate. On closer inspection, the probable cause of this discrepancy becomes clear. Introducing the second critical speed did indeed improve the unbalance estimation, in the same way as for the foundation estimation, as can be seen from the difference in estimated residual unbalance between runs 7 and 8. The reason for the consistently large errors in unbalance estimation is due to the actual physical configuration of the rotor: since the two balance disks were separated by a distance of only 1·0 mm, they are effectively acting in the same plane. Table 5 shows that the estimated unbalance angles for disks A and B for these

TABLE 6

Identified foundation parameters for different rotor configurations

Estimated parameter	Foundation/direction (measured value)	Estimated mean value (S.D.)	Error (%)
Stiffness (N/m)	Ax (17 212)	15 573 (1138)	−9
	Ay (17 707)	17 649 (1393)	0
	Bx (17 277)	16 988 (560)	−2
	By (17 523)	16 910 (411)	−3
Mass (kg)	Ax (0·356)	0·372 (0·098)	4
	Ay (0·356)	0·396 (0·119)	11
	Bx (0·352)	0·393 (0·055)	12
	By (0·352)	0·377 (0·038)	7
Damping (N s/m)	Ax	7·19 (3·98)	—
	Ay	−4·76 (10·73)	—
	Bx	−2·27 (3·61)	—
	By	5·98 (7·68)	—

cases are approximately 180° out of phase, thus having the effect of cancelling out the unbalance magnitudes of the two disks.

The results presented in this subsection highlight several important facts. Firstly, for accurate unbalance and foundation identification to be performed, it is important for the response data used in the method to contain sufficient information. For the two-balance plane cases used here, it was necessary for two critical speeds to be included in the rotor running speed range before acceptably accurate results were obtained. Secondly, the physical selection of balance planes has also been shown to have a significant influence on the unbalance estimation. If these planes are chosen too close together then they effectively act at a single plane and cause inaccurate results. This problem should not arise in turbomachinery, however, where balance planes are usually well separated. It should also be noted that the foundation estimation did not suffer as a result of the balance plane specification and consistently accurate foundation parameter estimation was achieved throughout runs 8–11. Indeed, Table 6 shows that, overall, the errors in foundation estimation, even with the poor estimates of run 7 included, were identified with a high degree of accuracy for all of the runs performed. These results inspire confidence in the robustness of the foundation identification for dealing with various rotor configurations, a lack of response information and a poor specification of balance planes.

4.2.2. *Different foundation configurations*

In order to test the capability of the identification method for dealing with changes in foundation configuration, the run-downs described in this section were performed with the changes in the mass of the bearing housings listed in Table 7, where the values of added mass are given in parantheses. This was felt to be a more demanding exercise than changing the foundation stiffnesses, since, as has been discussed above, mass identification is more sensitive to error than stiffness identification. The rotor configuration used for these cases was virtually identical to that used for configuration C2 in the previous section and the frequency range of 42–15 Hz was used—a range including both critical speeds. Runs 12–14 were all performed with the rotor in its residual unbalance state. There was not considered

TABLE 7

Changes made to foundation masses

Run	Total mass (kg)	
	Foundation A	Foundation B
12	0·436 (0·080)	0·432 (0·080)
13	0·356	0·432 (0·080)
14	0·356	0·512 (0·160)

TABLE 8

Identified unbalance parameters: various foundation configurations

Run	Disk	Estimated unbalance (g @ deg)
12	A	0·9@76
	B	2·2@96
13	A	0·9@75
	B	2·1@97
14	A	1·0@76
	B	2·1@96

to be any advantage in performing additional runs using trial weights to check the accuracy of the unbalance identification, since this has already been thoroughly examined. The identified residual unbalance parameters are, nevertheless, given in Table 8. The identified foundation parameters are given in Table 9.

The unbalance parameters of Table 8 do not exhibit any significant differences throughout the three run-downs performed. The maximum variations in estimated unbalance magnitude and phase angle are 0·1 g and 1° respectively. This shows that the unbalance identification is not significantly affected by physical changes to foundation parameters.

For the identification of the flexible supporting structure, the stiffnesses are identified consistently, with mean values and standard deviations (given in parantheses) of 17 476 (168), 18 592 (96), 16 420 (162) and 17 101 (129) N/m, for Ax, Ay, Bx and By respectively, corresponding to very low errors of 2, 5, −5 and −2%. For damping, these values are 7·37 (1·07), 4·71 (0·93), −0·30 (0·36) and −0·18 (0·25) N s/m. For mass identification, the results for foundation B, where the mass was varied in each of the three runs, are very encouraging, with a maximum error of 8% in the vertical direction for run 14. For foundation A, although the estimated errors in total mass are relatively high (as found previously), the estimated added mass between runs 12 and 13 is much more accurate at around 15%. These results are promising, in the sense that the added mass has been accurately estimated, even though the absolute mass estimation of foundation A is subject to some error.

The results presented in this section have highlighted the ability of the foundation and unbalance identification method to cope with changes in physical system parameters.

TABLE 9

Identified foundation parameters: various foundation configurations

Run	Estimated foundation parameters (Ax, Ay, Bx, By)			
	Mass (kg)	Error in mass (%)	Stiffness (N/m)	Damping (N s/m)
12	0·572	31	17 408	6·20
	0·566	30	18 564	4·63
	0·445	3	16 527	− 0·05
	0·454	5	17 052	− 0·08
13	0·479	34	17 354	8·30
	0·474	33	18 513	3·83
	0·428	− 1	16 233	− 0·72
	0·454	5	17 003	0·01
14	0·491	38	17 668	7·61
	0·486	36	18 699	5·68
	0·532	4	16 500	− 0·14
	0.554	8	17 248	− 0.46

Several rotor configurations have been tested, which showed the importance of selecting both a suitable speed range and a sensible set of balance planes to enable accurate results to be obtained. The method has also been shown to be suitably robust to changes in both rotor and foundation configuration.

4.3. IDENTIFYING ALTERNATIVE PARAMETER SETS

So far, none of the identified foundation parameter sets, as defined in equation (20), have included any cross-coupling terms. Since the foundations are of a relatively straightforward design, with no complicated coupling, this was considered an adequate choice of parameters, as has been proven by their accurate identification. The aim of the work described in this section was to study the effects of using different foundation parameter sets on the identification method. Although the specification of foundation parameters will always depend on the system in hand, this was felt to be an interesting and useful exercise, which should provide guidelines for future use of the method. The data obtained from run 17 (initial rotor configuration) were used as a test case. There was no particular reason for using this set of data—it simply serves as an example. The various parameter sets used are listed in Table 10. Only the foundation stiffness matrices are shown, for the sake of clarity, but the same form was also used for mass and damping, except for set 6, where the mass and damping matrices were constrained as diagonal. All of the matrices were symmetric. The only changes required to the method were the alternative specifications of equation (20), which were easily incorporated into the analysis. In order to predict the effect of the different parameter sets on the accuracy of the estimated results, the singular values and corresponding condition number of the regression matrix of equation (23) were first obtained, for each different set of parameters. Using this information, it was then possible to estimate the number of variables able to be successfully identified. These results are shown in Figures 8 and 9, which suggest that using parameter sets 1 (diagonal) and 3

TABLE 10

Alternative foundation parameter sets

Set	Parameter specification	Description
1	$\begin{bmatrix} K_{Ax,Ax} & & & \\ & K_{Ay,Ay} & & \\ & & K_{Bx,Bx} & \\ & & & K_{By,By} \end{bmatrix}$	No cross-coupling terms present As used previously
2	$\begin{bmatrix} K_{Ax,Ax} & 0 & K_{Ax,Bx} & 0 \\ & K_{Ay,Ay} & 0 & K_{Ay,By} \\ & & K_{Bx,Bx} & 0 \\ & & & K_{By,By} \end{bmatrix}$	Cross-coupling between foundations in the same direction, but not between directions
3	$\begin{bmatrix} K_{Ax,Ax} & K_{Ax,Ay} & 0 & 0 \\ & K_{Ay,Ay} & 0 & 0 \\ & & K_{Bx,Bx} & K_{Bx,By} \\ & & & K_{By,By} \end{bmatrix}$	Cross-coupling between directions at each foundation, but not between foundations
4	$\begin{bmatrix} K_{Ax,Ax} & K_{Ax,Ay} & K_{Ax,Bx} & 0 \\ & K_{Ay,Ay} & 0 & K_{Ay,By} \\ & & K_{Bx,Bx} & K_{Bx,By} \\ & & & K_{By,By} \end{bmatrix}$	Cross-coupling between foundations in the same directions and directions at each foundation (combination of 2 and 3)
5	$\begin{bmatrix} K_{Ax,Ax} & K_{Ax,Ay} & K_{Ax,Bx} & K_{Ax,By} \\ & K_{Ay,Ay} & K_{Ay,Bx} & K_{Ay,By} \\ & & K_{Bx,Bx} & K_{Bx,By} \\ & & & K_{By,By} \end{bmatrix}$	Fully cross-coupled between both bearings and in both directions
6	As 5 but with diagonal mass and damping matrices	

(cross-coupling between directions at each foundation) would deliver accurate solutions, indicated by the low condition numbers and cut-off points for the singular values. The condition number for parameter set 2 (cross-coupling between foundations in the same direction) is significantly lower than for sets 4–6 but significantly higher than for sets 1 or 3. It was expected that these results might also be of interest. Inaccurate results could be expected from sets 4–6, with high condition numbers. Set 1 will be assumed as the control set, since these results have already been shown to give close agreement with known unbalance and foundation parameters. The identified unbalance parameters for the different sets are listed in Table 11, where the error is relative to the control set. The matrices shown in Table 12 contain the estimated stiffness and mass parameters obtained using the different parameter sets. For the sake of clarity, the damping matrices have not been included—as has been seen throughout the previous results, they exhibit the same patterns of behaviour as the stiffness and mass matrices.

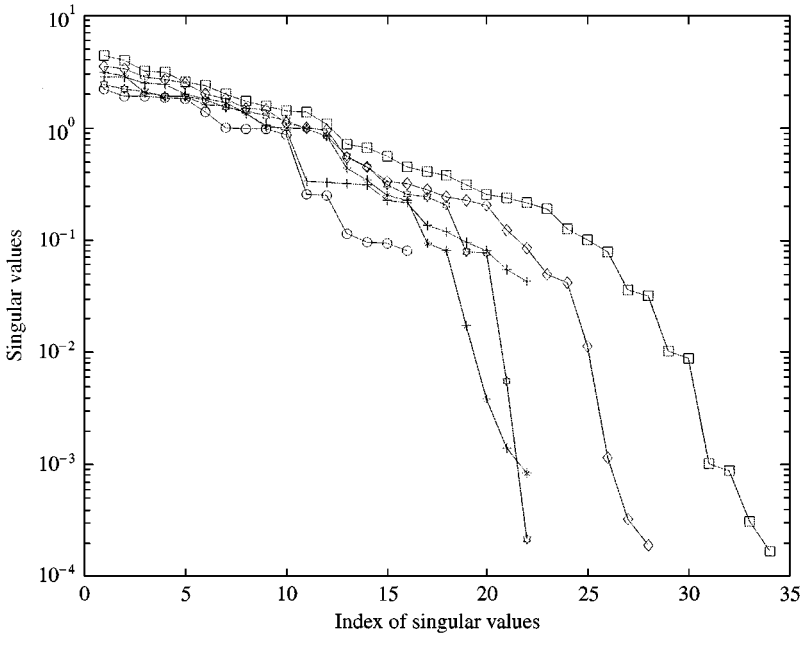

Figure 8. Singular values of regression matrices: parameter sets 1–6. —○—, set 1; —∗—, set 2; —+—, set 3; —◇—, set 4; —□—, set 5; —☆—, set 6.

Taking into account both the identified unbalance and foundation parameters for the various parameter sets, it is evident that the above predictions, made using the singular value and condition number information, were correct. The results for each individual case are discussed below:

Set 1 (*diagonal matrices*): The condition number for set 1 is very low and highly accurate results are obtained. This is the control set against which other results are compared, and is considered an accurate representation of the physical system.

Set 2 (*cross-coupling between foundations in the same direction*): The condition number here is significantly higher than for set 1. Interestingly, both the identified foundation and unbalance parameters are very accurate for foundation B and disk B respectively, whilst very inaccurate for foundation A and disk A (large and negative cross-coupled terms are identified for foundation A). The reason for the less accurate identification for disk A and foundation A may be numerical (the condition number in this case is relatively high), or due to the sensitivity of foundation A to modelling error. In a physical sense, such coupling is quite unlikely in this particular system.

Set 3 (*cross-coupling between directions at each foundation*): This is probably the most physically realistic specification of all the alternative foundation parameter sets investigated in this study. Directional cross-coupling at individual foundations is much more likely than cross-coupling between foundations. The estimates for this set, as predicted above, show no significant error for both the foundations and for the unbalance. The estimated cross-coupled terms are very small, as was expected.

Sets 4–6: The results obtained for the last three sets are all consistently poor. No improvement is shown when constraining the mass and damping matrices to be diagonal (set 6). These results agree with the predictions made above. None of these parameter sets are physically likely for the experimental system used in this work.

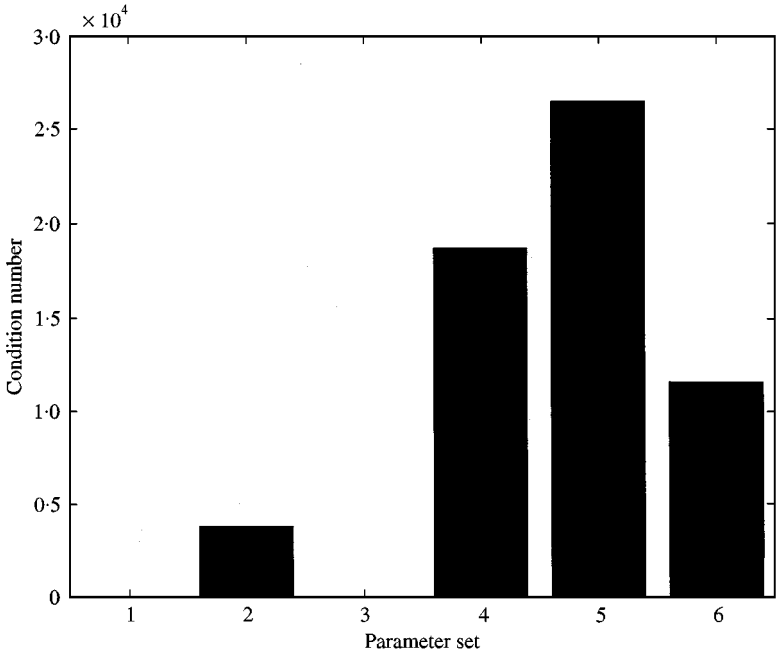

Figure 9. Condition numbers of regression matrices: parameter sets 1–6.

TABLE 11

Identified unbalance parameters: parameter sets 1–6

Set	Estimated unbalance	Error in unbalance
	Disk A; Disk B (g @ deg)	
1	1·2@17 1·8@275	Control set
2	3·3@53 2·0@261	2·1@36 0·2@ − 14
3	1·2@17 1·8@274	0·0@0 0·0@ − 1
4	0·3@122 0·4@279	−0·9@105 −1·4@4
5	0·3@121 0·4@279	−0·9@104 −1·4@4
6	0·7@136 0·6@283	−0·5@119 −1·2@8

These results are encouraging for two principal reasons. Firstly, they verify the predictions made above, giving confidence in the method of inspecting singular values and condition numbers to anticipate the behaviour of the identification. They also show that, for the system used here, as well as diagonal foundation matrices, the physically viable

TABLE 12

Estimated stiffness and mass parameters: parameter sets 1–6

Set	Estimated stiffness matrix (N/m)	Estimated mass matrix (g)
1	$\begin{bmatrix} 17231 & & & \\ & 18812 & & \\ & & 16832 & \\ & & & 16803 \end{bmatrix}$	$\begin{bmatrix} 453 & & & \\ & 470 & & \\ & & 365 & \\ & & & 360 \end{bmatrix}$
2	$\begin{bmatrix} 6469 & 0 & -5348 & 0 \\ & 7536 & 0 & -5470 \\ & & 16860 & 0 \\ & & & 16827 \end{bmatrix}$	$\begin{bmatrix} -102 & 0 & -308 & 0 \\ & -94 & 0 & -312 \\ & & 363 & 0 \\ & & & 360 \end{bmatrix}$
3	$\begin{bmatrix} 16788 & 1000 & 0 & 0 \\ & 18592 & 0 & 0 \\ & & 17070 & -396 \\ & & & 16920 \end{bmatrix}$	$\begin{bmatrix} 447 & 39 & 0 & 0 \\ & 459 & 0 & 0 \\ & & 370 & -13 \\ & & & 364 \end{bmatrix}$
4	$\begin{bmatrix} -35254 & 181 & 12738 & 0 \\ & -35310 & 0 & 12462 \\ & & -5462 & -396 \\ & & & -5395 \end{bmatrix}$	$\begin{bmatrix} -1100 & 8 & -186 & 0 \\ & -1108 & 0 & -197 \\ & & -237 & -2 \\ & & & -240 \end{bmatrix}$
5	$\begin{bmatrix} -35071 & 404 & 12693 & -74 \\ & -35482 & -98 & 12769 \\ & & -5304 & 87 \\ & & & -5445 \end{bmatrix}$	$\begin{bmatrix} -1095 & 14 & -186 & 0{\cdot}1 \\ & -1105 & -0{\cdot}6 & -188 \\ & & -233 & 0{\cdot}1 \\ & & & -238 \end{bmatrix}$
6	$\begin{bmatrix} -40453 & -220 & 20136 & 70 \\ & -42017 & -57 & 20715 \\ & & -8347 & 115 \\ & & & -8844 \end{bmatrix}$	$\begin{bmatrix} -1077 & & & \\ & -1113 & & \\ & & -248 & \\ & & & 261 \end{bmatrix}$

representation including cross-coupling between directions at each foundation may be used with no significant reduction in accuracy. For future work using this identification method, this prediction technique is therefore recommended.

4.4. BEND IDENTIFICATION

To fully investigate the inclusion of bend excitation in this experimental study, two main tasks were accomplished. Firstly, the identification was performed, assuming both bend and

unbalance excitation, on a previously obtained set of data, where a straight rotor was used and only unbalance forcing was present. This was done to check for differences between the method assuming unbalance excitation alone and when assuming both bend and unbalance excitation. The effect of including various numbers of modes in the bend representation has also been examined. Secondly, a bent rotor was used in the experiment and the identification method again performed using the two assumed excitation sources. As well as the bend identification itself, the differences in results obtained when using the two different forms of assumed excitation have been examined.

4.4.1. *Bend identification with pure unbalance excitation*

The data obtained from runs 17 and 18 (initial rotor configuration) were used for this study. The rotor was in its residual unbalance state for run 17 and trial weights were added to both disks for run 18. The identification was performed on the data for both run-downs, allowing varying numbers of modes to be included in the bend representation. A minimum of 1 and maximum of 6 modes (in each perpendicular direction) were allowed. The *unbalance only* results are also given, to allow the results including both *bend and unbalance* to be compared. The unbalance identification results for the various cases are given in Table 13. There is no significant change in either unbalance magnitude or phase angle estimation when including the bend, for all modes used. The same behaviour was also exhibited for the identified foundation parameters. There is negligible variation between the stiffness, mass and damping estimates for all numbers of modes for both runs 17 and 18. The estimated mass and stiffness parameters are all identified to the same, high degree of accuracy as was achieved for the *unbalance only* case.

The estimated bend profiles, for both runs and for all six cases, are shown in Figure 10. The first fact to be gathered from the various profiles is that they are all significantly different, in terms of either shape and/or magnitude. Since the estimated unbalance and foundation estimates were accurate in all six cases for both runs, then a decision must be made about how many modes should be included in the analysis to give realistic results, i.e., which of the estimated profiles in Figure 10 is most accurate? Obviously, the estimates using 5 or 6 modes can be immediately discounted. The magnitude of the bend in both of these cases is extremely large and makes no physical sense, considering the rotor was not intentionally deformed before these run-downs and should therefore have been virtually straight. Also, there is little consistency between these estimated profiles for the two runs considered. When 3 or 4 modes are used, there is good consistency between the two runs. However, the magnitude and relatively complicated shapes of the profiles estimated in these cases make the results difficult to believe. For modes 1 and 2, the low magnitudes, overall shapes and good consistency between the two runs make either of these cases seem likely. For the case with 2 modes, the difference between the maximum and minimum bend amplitudes is less than 0·02 mm. Since this kind of profile amplitude would easily be possible in such a system, and since it would seem sensible to include as many modes in the bend modal representation as are in the running range of the machine, 2 modes will be used for the bend identification described in the following section. Further investigation would be necessary to determine whether using as many modes as are in the running range is a reasonable generic guideline, but for the system used here, this seems a sensible path to follow. This may be verified in the following work, where a known bend profile is to be identified.

4.4.2. *Bend identification with both bend and unbalance excitation*

To achieve excitation due to a bent rotor, of similar magnitude as that due to residual unbalance, a shaft supported at both ends was placed in a hydraulic press and subjected to

TABLE 13

Estimated unbalance parameters: various modal representations

No. of modes	Run	Unbalance (disk A; disk B; mass (g) @ deg)		
		Configuration	Calculated addition	Error
No bend	17	Residual		
	18	1·2@11	1·3@24	0·1@13
		1·8@281	1·7@304	−0·1@23
1	17	Residual		
	18	1·2@11	1·4@23	0·2@12
		1·8@281	1·7@305	−0·1@24
2	17	Residual		
	18	1·2@11	1·4@20	0·2@9
		1·8@281	1·7@304	−0·1@23
3	17	Residual		
	18	1·2@11	1·4@18	0·2@9
		1·8@281	1·7@305	−0·1@24
4	17	Residual		
	18	1·2@11	1·4@18	0·2@9
		1·8@281	1·7@305	−0·1@24
5	17	Residual		
	18	1·2@11	1·4@18	0·2@9
		1·8@281	1·7@305	−0·1@24
6	17	Residual		
	18	1·2@11	1·4@18	0·2@9
		1·8@281	1·7@305	−0·1@24

an incrementally applied mid-span load, until the required bend amplitude was achieved. Two run-downs were performed between 45 and 15 Hz, one with the rotor in its residual unbalance state and the second with trial weights added to both disks. The rotor configuration used was very similar to that of configuration C2, described above. The foundations were also in their original configurations, i.e., with no added mass. The identification method was performed twice for each set of response data: once with *unbalance only* excitation assumed, and again with both *bend and unbalance* excitation assumed. A description of the various sets of results is given in Table 14.

Some variation was shown for the foundation estimates, both between the two different runs and between the two different assumed excitation sources, although the overall accuracy in estimated parameters was reasonable. The most significant discrepancies were for the mass and stiffness estimation of foundation A, which is less consistent than for foundation B. For sets 1 and 3, which one would expect to be the most accurate, since these sets have both types of excitation assumed, the largest error is 38% in the stiffness estimation for the horizontal direction at foundation A. The least-accurate results are for set 4, although this does not give cause for concern, since this set had *unbalance only* excitation assumed for identification purposes, which is not a physically accurate representation of the system.

The unbalance estimation results are given in Table 15. Although the actual *estimated unbalance* varies considerably between sets 1 and 2 (residual) and sets 3 and 4 (trial weights), the estimated *added unbalance* for both sets remains accurate, with low errors in both

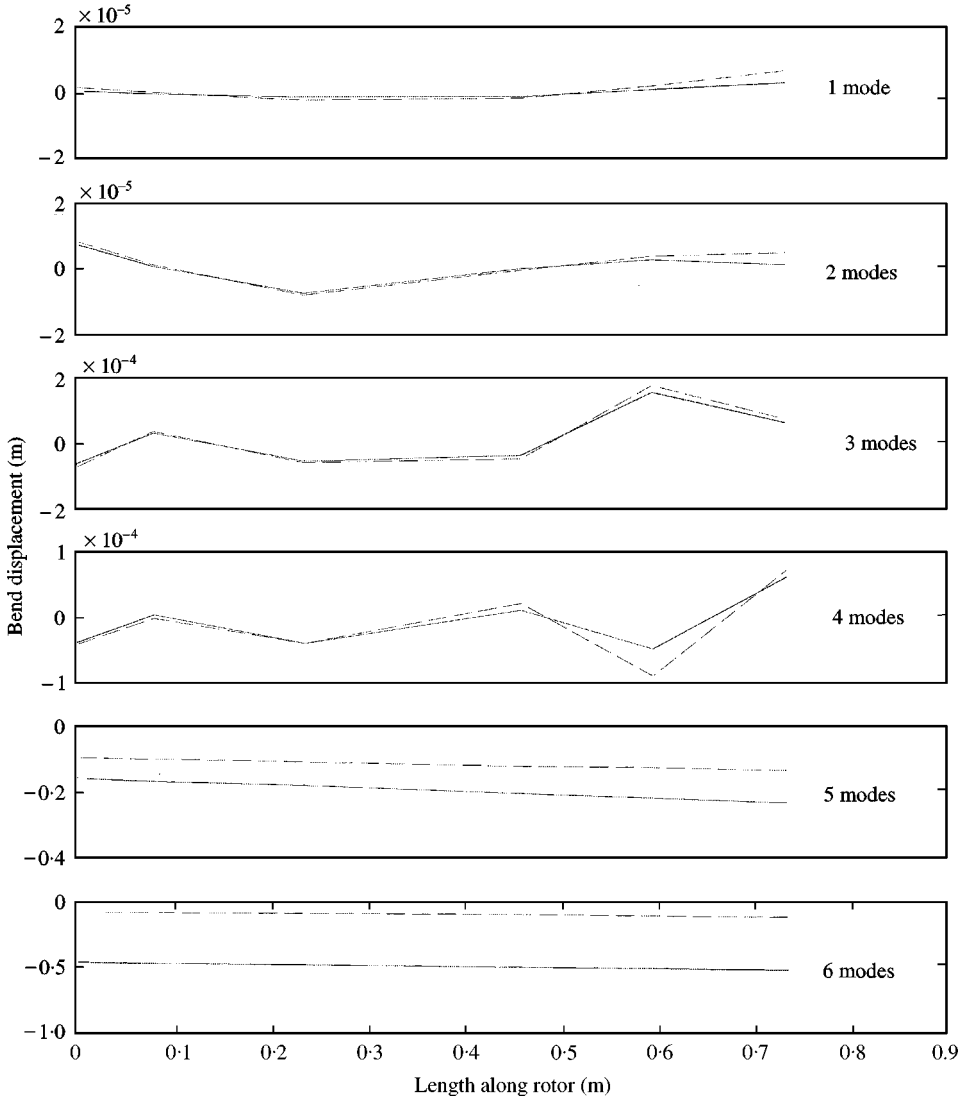

Figure 10. Estimated bend profiles (total amplitude): various modal representations, (——, run 17; – – –, run 18).

magnitude and angle estimation. This implies that the *unbalance only* identification method is robust enough, in this instance, to predict the added unbalance. This is plausible, since only the unbalance forcing was changed between the two runs and should therefore be detectable. However, the actual state of unbalance from a single run cannot be accurately predicted assuming *unbalance only* excitation: for this to be achieved, the bend excitation must also be included in the analysis. In addition, the estimated unbalance (*unbalance only case*) is significantly higher for three out of the four estimated results. These higher estimates compensate for the extra forcing provided by the bend, unaccounted for by the identification method, and thus attributed to unbalance excitation. Once the bend forcing is included in the analysis, these values become lower, since this extra forcing is then rightly provided by the bend. It is therefore important to include the bend excitation, to allow

TABLE 14

Description of results sets used for bend experiment

Set	Description (assumed excitation)
1	Residual run: (unbalance and bend)
2	Residual run: (unbalance only)
3	Trial weights run: (unbalance and bend)
4	Trial weights run: (unbalance only)

TABLE 15

Unbalance identification results: bend experiment

		Unbalance (disk A; disk B; mass (g) @ deg)		
Set	Configuration	Estimated	Calculated addition	Error
1	Residual	1·0@153	—	—
		2·1@57	—	—
2		1·7@181	—	—
		3·2@50	—	—
3	1·8@349	1·0@54	1·5@14	−3·0@25
	2·0@236	1·0@349	2·0@264	0·0@28
4		0·3@106	1·6@12	−0·2@23
		1·6@14	2·1@258	0·1@22

accurate unbalance estimates to be calculated, and therefore to balance the rotor successfully from a single run-down.

The estimated and measured bend profiles are shown in Figure 11. The bend was measured by very slowly turning the rotor and measuring the displacement amplitude with a dial gauge at axial locations corresponding to the nodes of the rotor model. The method was subject to a certain amount of error due to difficulties in positioning the gauge on the rotor, but this was not considered to detract from the overall accuracy of the measurements taken.

The estimated bend profiles show much promise for the practical application of the bend identification method. It should first be noted that the estimated profiles for both runs (with residual and added unbalance respectively) exhibit excellent consistency. This shows that the method can distinguish between the two types of forcing present in this experiment, since the added masses of the second run were accurately identified, whilst the estimated bend profiles remained constant when the mass was added. Thus, the method has been shown to differentiate between the forcing produced by the bend and that produced by pure mass unbalance. The estimated bend profile is of the same general shape and magnitude as has been measured. Indeed, all but two of the estimated values show excellent agreement with their measured values: the poorer estimates are for those two points at the free end of the rotor. The reason for this may be that, since the free end is less strained than the driven

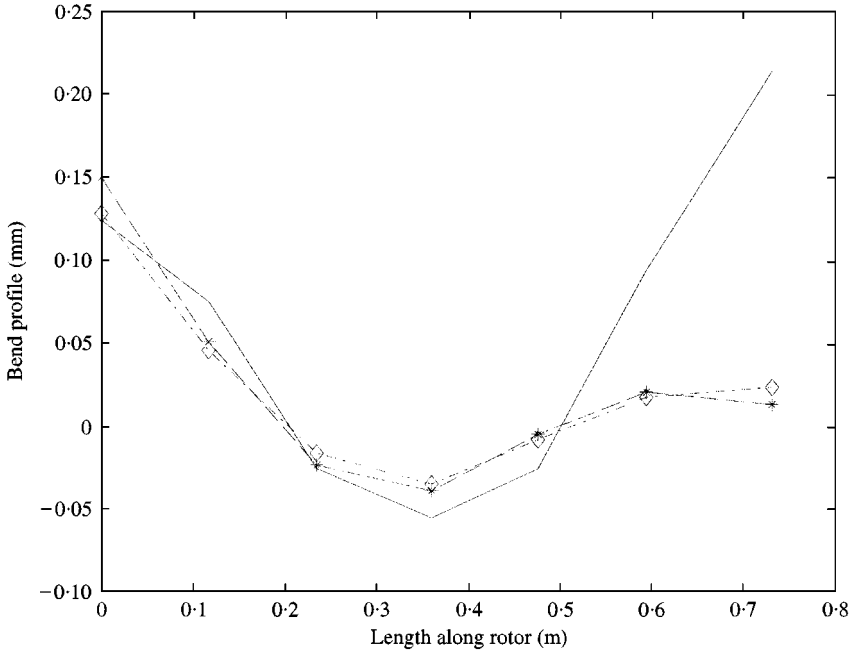

Figure 11. Measured and estimated bend profiles (total indicated reading): ——, measured; – – × – –, estimated, residual; – –◇– –, estimated; trial weights.

end, the bend at the free end does not have as much of an effect on the response. Nevertheless, the fact that the overall bend profile has been consistently accurately identified, together with accurate foundation and added unbalance parameters, is very encouraging for the identification method presented in this work.

5. SUMMARY AND CONCLUSIONS

An identification method for estimating both the excitation and flexible support parameters of a rotor-bearings-foundations system has been presented. Excitation due to both mass unbalance and a bent rotor was included in the analysis, which has been verified experimentally. The method has great practical potential, since it allows balancing to be performed on a rotor using data obtained from just a single run-up or run-down of the machine, which has obvious benefits for the efficient operation of machinery in the field. Using this single-shot balancing technique, vibration levels of an experimental rotor rig were successfully reduced by as much as 92% of their original levels. A bend in a rotor has been accurately identified in this work. It was also shown that including bend identification in those cases where only unbalance forcing was present in no way detracted from the accuracy of the estimated unbalance and foundation parameters. To avoid confusion between these two types of forcing, thus allowing balancing to be performed more efficiently, it is recommended that the form of the method including bend excitation be used. The identification of flexible foundation parameters has been successfully achieved, with measured and estimated parameters matching very closely in most cases. The identification method was tested for a wide range of conditions, and proved suitably robust to changes in

system configuration, noisy data and modelling error. The experimental results were very encouraging for the method and it is envisaged that the main thrust of future work on this topic should be the application of the identification method to larger, more complicated machines, and eventually to power station turbogenerators.

ACKNOWLEDGMENTS

The authors are pleased to acknowledge the support of BNFL (Magnox Generation) and the Engineering and Physical Sciences Research Council. Dr Friswell gratefully acknowledges the support of the EPSRC through the award of an Advanced Fellowship.

REFERENCES

1. A. G. PARKINSON 1991 *Proceedings of the Institution of Mechanical Engineers Part C—Journal of Mechanical Engineering Science* **205**, 53–66. Balancing of rotating machinery.
2. A. W. LEES 1998 *Proceedings of the Institution of Mechanical Engineers—Vibrations in Rotating Machinery Paper* C306/88, 209–216. The least squares method applied to identify rotor/foundation parameters.
3. A. W. LEES and M. I. FRISWELL 1997 *Journal of Sound and Vibration* **208**, 671–683. The evaluation of rotor unbalance in flexibly mounted machines.
4. J. C. NICHOLAS, E. J. GUNTER and P. J. ALLAIRE 1976 *Journal of Engineering for Power* **98**, 171–181. Effect of residual shaft bow on unbalance response and balancing of a single mass flexible rotor. Part 1—unbalance response.
5. J. C. NICHOLAS, E. J. GUNTER and P. J. ALLAIRE 1976 *Journal of Engineering for Power* **98**, 182–189. Effect of residual shaft bow on unbalance response and balancing of a single mass flexible rotor. Part 2—balancing.
6. A. JENNINGS and J. J. MCKEOWN 1993 *Matrix Computation*. Chichester: Wiley (second edition).